This article has been accepted for inclusion in a future issue of this journal. Content is final as presented, with the exception of pagination.

Sparse Reconstruction-Based Thermal Imaging for Defect Detection

Deboshree Roy, Prabhu Babu, and Suneet Tuli

***Abstract*— This paper proposes an idea of employing sparse reconstruction-based technique for thermal imaging defect detection. The implementation of the reconstruction technique is tested on a carbon fiber reinforced polymer test piece with artificially drilled defects and the test results are compared with the established cross correlation method. The two processes are compared in terms of defect detectability, their SNR variation with defect depth and their computation complexity. When compared with cross correlation algorithm, the technique is expected to solve memory space problems by compressing all information from large cross-correlated pulse video into a single reconstructed image as an output. Furthermore, in existing cross correlation methods, the pulse peak time shifts with defect depth. Hence, defect quantification algorithms, such as SNR calculation, require multiple frame analysis. Such algorithms are comparatively simplified in sparse reconstruction technique. This paper explores sparse reconstruction algorithm for resolving close-spaced defects. This paper further describes cross-validation method for optimization of a user parameter in sparse reconstruction method.**

***Index Terms*— Cross correlation algorithm, frequency modulated thermal wave imaging, nondestructive evaluation and remote sensing, pulse compression, sparse reconstruction, thermal nondestructive testing.**

I. Introduction

THERMAL imaging for defect detection is a technique where a presence of defect is indicated by a rise in temperature. Subsurface defect detection usually employs an external heating mode and is known as active thermography. Different active thermography techniques are lock-in thermography, frequency modulated thermography, and pulse thermography. Lock-in thermography utilizes a periodic photothermal heating scheme at a given frequency. The resultant change in temperature of the test piece is recorded and processed for defect detection [1], [2]. Frequency modulated thermal wave imaging utilizes a frequency modulated heating scheme where a band of frequency is incident on a sample [3]. An objective comparison of aforementioned active thermography methods is presented by Chatterjee *et al.* [4]. Pulse compression is a postprocessing technique used in conjunction with frequency modulated excitation scheme [5]. Pulse compression in the area of thermal wave imaging for defect detection is described in [6]–[8]. Pulse compression method is based on correlating the thermal response with a reference signal. Reference signal is an exact representation of excitation signal and used to generate the correlated pulse. The significance of reference signal and its acquisition methods are described in [9].

Pulse compression or cross correlation method has an advantage of an improvement in SNR by a factor of time-bandwidth product [5]. However, the presence of sidelobes in the signal degrades the thermal detection system. Furthermore, Roy and Tuli [10] show that a rise in time-bandwidth product does not improve the defect detection. Hence, alternate techniques are explored. Sparse reconstruction is expected to overcome the aforementioned shortcomings by minimizing the elements of reconstructed signal to zero.

Furthermore, each of the aforementioned techniques generates a video output with a large memory space. A memory efficient nonuniform data acquisition method was suggested in [10]. However, the data had to be interpolated to large uniform data for processing. Hence, a requirement for a memory efficient processing tool arises. A sparse reconstruction tool is expected to generate a single image output, thus compressing all information from a video into a single image. This, in turn, is expected to simplify the defect quantification and analysis. Sparse reconstruction is thus a useful tool and has found numerous applications are found [11]–[14].

Active thermography technique suffers from thermal diffusion resulting in a blurred defect edge and requires additional tool for defect size estimation [16]. The use of full-width half-maxima of a defect to determine its size for a pulse thermography experiment is described by Almond and Lau [15]. However, the technique is invalid for small defects. The role of sparse reconstruction algorithm in such applications is explored in this paper. The reconstruction algorithm is reported to resolve closely spaced objects by Charbonneir *et al.* [17], Yang and Li [18], Ye *et al.* [19], and Soldovieri *et al.* [20], particularly for SAR by Hasankhan *et al.* [21] and Zhu *et al.* [22]. Furthermore, it is an efficient tool nondestructive testing techniques [23]–[25].

Quadratic frequency modulation as an excitation signal is described in this paper. Different quadratic modulation signal generation techniques are described by O'Shea [26]. Ghali and Mulaveesala [28] describe quadratic frequency modulation in thermal imaging defect detection and compare the method with established linear frequency modulation as an excitation signal. Yoon *et al* [27] report that

Manuscript received August 2, 2018; revised November 28, 2018; accepted December 3, 2018. The Associate Editor coordinating the review process was Emanuele Zappa. *(Corresponding author: Deboshree Roy.)*

The authors are with the Centre for Applied Research in Electronics, IIT Delhi, New Delhi 110016, India (e-mail: deboshree_roy22@yahoo.com).

Color versions of one or more of the figures in this paper are available online at http://ieeexplore.ieee.org.

Digital Object Identifier 10.1109/TIM.2018.2889364

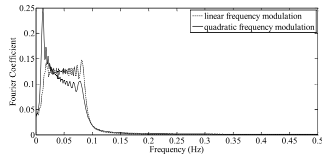

Fig. 1. Fast fourier transform of linear and quadratic frequency modulated signal.

generated compressed pulse has lower sidelobes, improved defect resolution, and more energy deposition in main lobe and hence is preferred over linear frequency modulation. Furthermore, the spectrum of quadratic frequency modulation depicted in Fig. 1 shows that energy is redistributed from high-frequency to low-frequency component by Subbarao and Mulaveesala [28] and Pecci *et al.* [29]. This facilitates deep defect detection. This paper proposes sparse reconstruction technique as a processing tool in thermal imaging defect detection. The method is developed as an alternate to an established cross correlation processing method. The two processes are compared in terms of defect detectability, their SNR variation with defect depth and their computation complexity. The variation in sparse reconstruction parameters such as computation time, l_0- and l_1-norms with user parameter α is described in this paper. This paper utilizes cross-validation as an optimization tool for α parameter. This paper further compares the two processing tools for apparent broadening in defect diameter. The cause of broadening of defect and role of sparse reconstruction in its removal has been described in this section.

II. Sparse Reconstruction Problem in Thermal Imaging Nondestructive Testing

Sparse approximation to signals deals with the problem of finding a representation of a signal as a linear combination of a small number of elements from a set of signals called dictionary in [30] and [31]. A signal is sparsely representable if there exists a sparsity basis $\{\psi_i\}$ with $R^{N\times M}$ dimensions, along with a discrete time observed signal of length N, $x(n), n = 1 \ldots . N$ and a sparse column vector θ of length M. The basis vectors are stacked as columns into $N \times M$ sparsity basis matrix $\psi = [\psi_1 \psi_2 \ldots . . \psi_M]$. In matrix notation

$$x = \psi\theta. \tag{1}$$

For $N \le M$, (1) is an overdetermined system and does not have a unique solution. A sparse solution is obtained under certain constraints. The basis pursuit (BP) solution to (1) is

$$\min_{\theta} \|\theta\|_1 \quad \text{s.t. } x = \psi\theta \tag{2}$$

where $\|\theta\|_1$ is the l_1-norm of θ. l_1-norm is defined as $\|\theta\|_1 = \sum_{i=1}^{N} |\theta(i)|$ and l_2-norm as $\|\theta\|_2 = (\sum_{i=1}^{N} |\theta(i)|^2)^{1/2}$. Similarly, $\|\theta\|_0$ is the l_0-norm, i.e., $\|\theta\|_0$ counts the number of nonzero entries in the vector θ. l_0-norm is the simplest and intuitive measure of sparsity in a signal. However, the l_0-norm function does not satisfy all the axiomatic properties of a true mathematical norm. The discrete and discontinuous nature of l_0-norm poses many challenges in its applications to recover sparse signals from their subsampled measurements [32]. Here, ψ is the N element dictionary. For a noisy x, the problem consists of

$$x = \psi\theta + \eta. \tag{3}$$

For a frequency modulated thermal imaging with sparse reconstruction, x in (3) is the measured signal, ψ is the time-shifted version of the reference signal, and η is the zero-mean additive white Gaussian noise with variance σ^2. The aim of sparse algorithm is to recover θ from x.

The solution to (3) of sparse reconstruction reduces to the following optimization problem:

$$\min_{\theta} \|x - \psi\theta\|_2^2 + \alpha\|\theta\|_1 \tag{4}$$

where α is a scalar quantity. Equation (4) is a convex optimization problem and is named as BP denoising (BPDN) by Chen *et al.* [33]. BPDN algorithm is based on least square minimization with l_1 regulariser. The regularizing term α determines the computational complexity and sparsity of the system by Gill *et al.* [34]. A small value of α restricts the parameters leading to sparser and more interpretable models that fit the input data. On the contrary, a large value of α frees the parameter and allows the model to adapt more closely to the training data. An optimum value of α is selected by cross-validation method by Bofonous *et al.* [35]. In the method, the data set is split into K number of groups. One group is fixed as a test set, and the remaining $(K-1)$ are the training set in [36] and [37]. The mean square error (MSE) of the algorithm is calculated at different α values. The method is repeated K times, with each K group acting as test set and the remaining $(K-1)$ group as the training set. These K number of MSE estimates are averaged for each α value to obtain the cross-validation error curve. The standard deviation of all errors is used to judge the model variation. A low value in standard deviation suggests that the model does not vary substantially with α. A high K value leads to high variance with less bias while a low value of K leads to more biased results. A balance between bias and variance is required. Leave one out cross-validation has a high variance and low bias. It is preferred for low computational complexity.

Least absolute shrinkage and selection operator (LASSO) is similar to BPDN but places a restriction on l_1-norm in [38] and [39] as depicted in (5). l_1-norm is concerned with the value of entries and not the quantity. A vector with a small l_1 value have numerous small-valued nonzero entries in every position that eventually results in large l_0-norm. A restriction in l_1-norm in LASSO generates sparse solution

$$\min_{\theta} \|x - \psi\theta\|_2^2 \quad \text{s.t. } \|\theta\|_1 \le \sigma. \tag{5}$$

where x, ψ, and θ represent the observed signal, dictionary, and sparse coefficients, respectively, and σ^2 represents the variance of additive white Gaussian noise in (3).

III. Problem Formulation

This paper describes and compares two different processing methods for defect detection; cross correlation and sparse

This article has been accepted for inclusion in a future issue of this journal. Content is final as presented, with the exception of pagination.

reconstruction techniques. The application of sparse reconstruction technique in the area of thermal imaging is studied in this paper and compared with an established cross correlation method.

A. Sparse Reconstruction

A brief background of sparse reconstruction has been presented in Section II. In (5), $x[n]$ depicts temperature response of the sample at a given pixel and is a column matrix of length N. ψ represents a recorded reference signal and η is the back-ground noise from the measurement system and material. The aim of the reconstruction technique is to minimize θ. ψ is a time-shifted version of reference signal with dimensions $N \times M$. Sparse reconstruction LASSO algorithm works individually on each pixels

$$\begin{bmatrix} x_1 \\ x_2 \\ \vdots \\ x_N \end{bmatrix} = \begin{bmatrix} \psi_1 & 0 & \dots & 0 \\ \psi_2 & \psi_1 & \dots & 0 \\ \vdots & \vdots & \ddots & \vdots \\ \psi_N & \psi_{N-1} & \dots & \psi_{N-M} \end{bmatrix} \begin{bmatrix} \theta_1 \\ \theta_2 \\ \vdots \\ \theta_M \end{bmatrix} + \begin{bmatrix} \eta_1 \\ \eta_2 \\ \vdots \\ \eta_N \\ . \end{bmatrix}$$

The LASSO problem is defined as

$$\min_{\theta} \|\widehat{x} - \widehat{\psi}\theta\|_2^2 + \alpha\|\theta\|_1 \tag{6}$$

where $\widehat{x} = (1-\alpha)^{1/2}x$ and $\widehat{\psi} = (1-\alpha)^{1/2}\psi$ and α varies from 0 to 1. In the above-mentioned equation, the scalar α is a user-selected parameter for l_1 minimization problem. The value of α determines the reconstruction accuracy and is basically a tradeoff between sparsity and reconstruction accuracy. It is optimized by tenfold cross-validation method, where the N set of observation is divided into $(N/100)$ test sets.

A tenfold cross-validation algorithm used in the experiment is described as follows.

1) A data is divided into 10 equal folds

$$x = [a_1|a_2|a_3|\dots|a_{10}] \tag{7}$$

where x is a matrix in (2) of dimensions $1 \times N$, and the folds are defined as $a_1, a_2 \dots a_{10}$, each of dimension $1 \times N/10$. ψ in (2), is similarly divided into 10 folds, each with dimension $N/10 \times M$.

2) For $k = 1$ to 10, each a_k is kept as validation set, and all remaining $k-1$ set is kept as training set.

3) Solve equation

$$\min_{\theta_{\mathrm{tr}}} \|x_{\mathrm{tr}} - \psi_{\mathrm{tr}}\theta_{\mathrm{tr}}\|_2^2 + \alpha\|\theta_{\mathrm{tr}}\|_1 \tag{8}$$

where x_{tr}, ψ_{tr}, and θ_{tr} represent the training set for cross-validation algorithm, derived from (4). Herein, x_{tr} represents the training set of the observed signal, ψ_{tr} is the training set of the dictionary, and θ_{tr} represents the sparse reconstructed signal, obtained from the training set parameters.

4) Solve equation

$$\min_{\theta_{\mathrm{val}}} \|x_{\mathrm{val}} - \psi_{\mathrm{val}}\theta_{\mathrm{val}}\|_2^2 + \alpha\|\theta_{\mathrm{val}}\|_1 \tag{9}$$

where x_{val}, ψ_{val}, and θ_{val} represent the validation set for cross-validation algorithm, derived from (4). Herein, x_{val} represents the validation set of the observed signal, ψ_{val} is the validation set of the dictionary, and θ_{val} represents the sparse reconstructed signal, obtained from the validation set parameters.

5) The cross-validation error, e for a tenfold cross-validation algorithm is defined as

$$e = \frac{1}{10}\sum_{k=1}^{10}(\theta_{\mathrm{val}} - \theta_{\mathrm{tr}})^2 \tag{10}$$

where e is the cross-validation error calculated using θ_{tr} and θ_{val}. They are the sparse reconstruction coefficient obtained from (4) and (10), respectively. The value of α is optimized by calculating e for all values of α and selecting α the minimum e. The α is optimized for each pixel individually by repeating the cross-validation algorithm.

TABLE I

THERMAL DIFFUSION LENGTH FOR CFRP. THE PARAMETER VALUES ([10]) USED ARE $k_{||} = 4$ W/m °C; $\rho = 1600$ kg/m^3; AND $c = 1200$ J/kg °C

Frequency (mHz)	Diffusion Length (mm)
10	8.1
90	2.7

B. Optimized α for Sparse Reconstruction Algorithm

Sparse reconstruction efficiency is based on an initial selected value of α. An algorithm is formulated for optimizing user parameter α. A sparsity-based algorithm is summarized in Algorithm 1 and described as follows.

1) For a given pixel location x, y, the LASSO problem described in (6) is solved.
2) A tenfold cross-validation method described in Section III-A is used at values of α varying between 0 and 1 with a step size of 0.1 for calculation of MSE in (10). α with minimum MSE is used for solving LASSO problem.
3) The entire algorithm is repeated for all pixel locations.

Algorithm 1 Sparse Reconstruction Algorithm With Optimized α

```
for all pixel location in x and y do
  for all α in 0.09 to 0.99 at an increment of 0.1 do
    (I) solve LASSO problem
    (II) define a tenfold cross-validation problem for calculation of e.
  end for
  select α with minimum e. repeat for all x and y pixels.
end for
```

The complete algorithm is repeated individually for each pixel for a final sparse reconstructed image. The algorithm is compared with cross correlation algorithm.

This article has been accepted for inclusion in a future issue of this journal. Content is final as presented, with the exception of pagination.

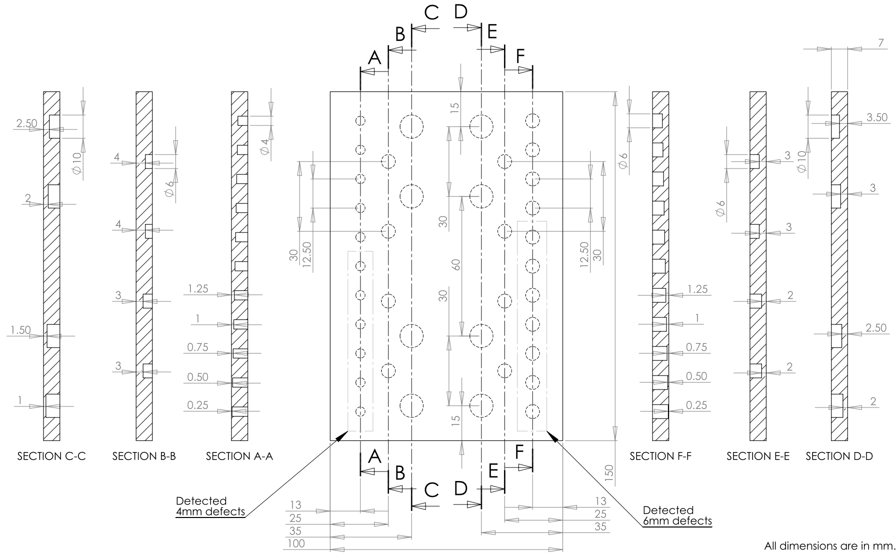

Fig. 2. CFRP sample.

C. Cross Correlation Method

The IR camera recorded video is processed with two processing techniques. The first one is a cross correlation technique, and the second one is a sparse reconstruction technique. The algorithm for cross correlation is as follows and described in detail in [9].

1) The time-temperature variation in the excited test piece comprises of an ac or oscillatory part and a dc part that depicts an average rise in temperature. The dc component in thermal response and reference signal is removed by polynomial fitting. The process is known as offset removal

$$T(x,y,t) = T_{\mathrm{ac}}\cos(\omega t) + T_{\mathrm{dc}}$$
$$T_{\text{dc-rem}}(x,y,t) = T(x,y,t) - \sum_{i=1}^{N} a_i(x,y)t^i \quad (11)$$

where $T_{\mathrm{ac}}(x,y,t)$ is the ac and T_{dc} is the dc part of the recorded temperature of test-piece. $T_{\text{dc-rem}}(x,y,t)$ is the offset removed temperature of the test piece at pixel (x,y). It represents only the ac component of the temperature.

2) The offset removed reference signal is cross-correlated in time domain with the thermal response signal for a resultant pulse compressed signal [9]

$$x_{\text{cross-corr}}[n] = \sum_{k=1}^{N} \psi[k] T_{\text{dc-rem}}[n-k]. \quad (12)$$

Here, in (12), x represents cross-correlated term, ψ represents reference signal, and $T_{\text{dc-rem}}$ represents the offset removed temperature response of the test piece.

The algorithm is applied individually to each pixels to generate pulse compressed video. The algorithm is based on removing the phase difference between excitation reference signal and thermal response of the test piece to generate a peak pulse [9]. The method, however, suffers from pulse broadening.

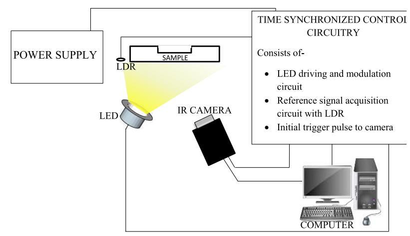

Fig. 3. Experimental setup diagram [10].

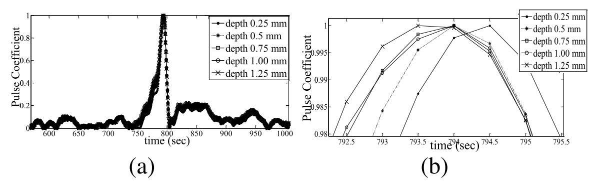

Fig. 4. Normalized timing diagram of compressed pulse for defects with varying depth and 6 mm diameter. (a) Full timing diagram. (b) Zoomed timing diagram.

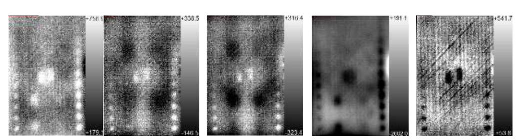

Fig. 5. Thermogram variation from compressed video with frame.

IV. Experiment

A. Excitation Signal

The excitation signal is a quadratic frequency modulated signal within a band of frequency from 0.01 to 0.09 Hz for a duration of 800 s. The excitation signal is depicted in the following equation:

$$x_{\mathrm{exc}}(t) = \mathrm{sgn}(\sin(2\pi(\phi(t))))$$
$$\phi(t) = 2*\pi\left(f_0 + \frac{k}{3}t^2\right)t$$
$$f(t) = \frac{d\phi}{dt} = 2\pi(f_0 + kt^2) \quad (13)$$

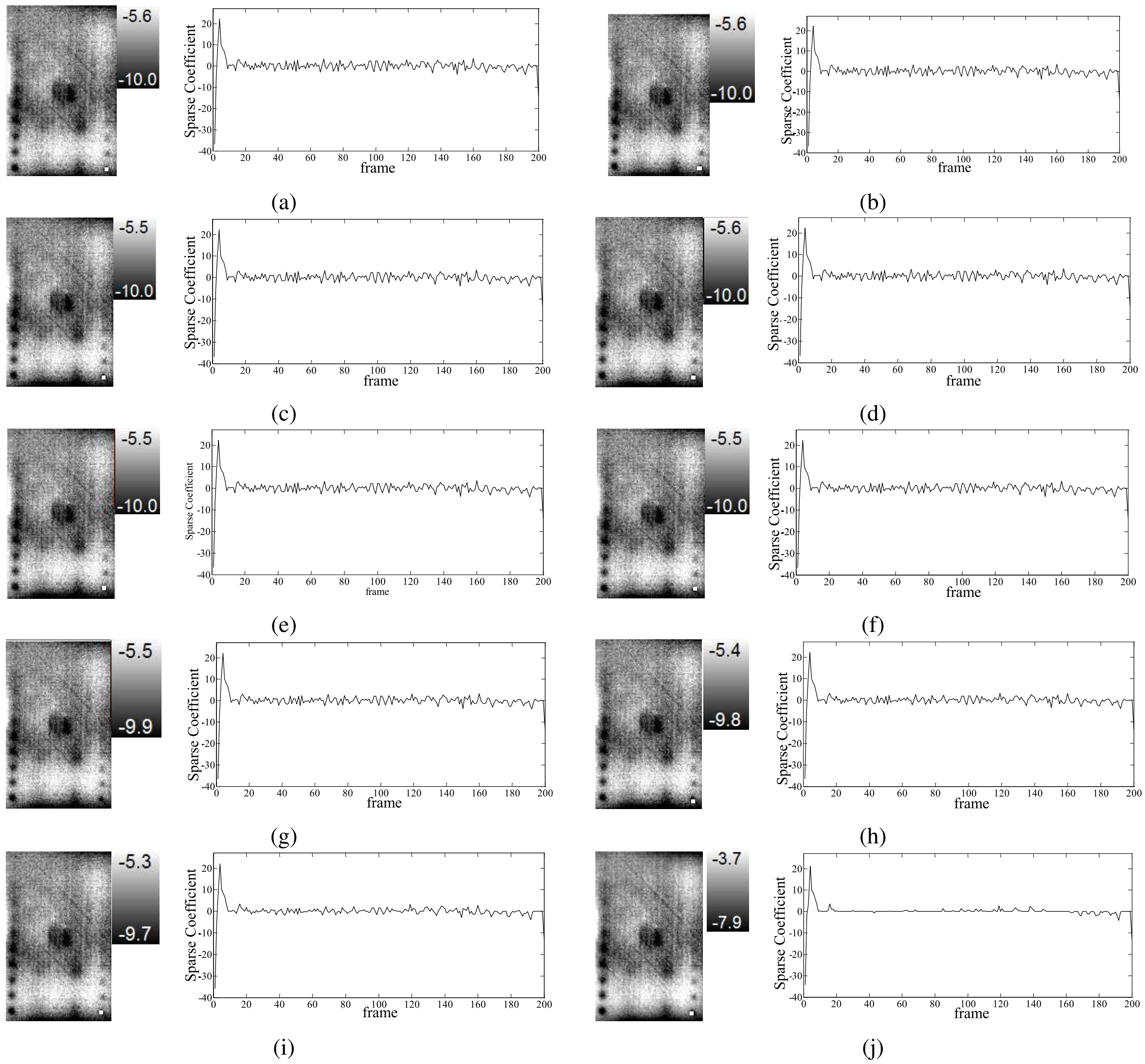

Fig. 6. Sparse reconstructed thermal images obtained at different α and sparse coefficient variation with time at a selected pixel. (a) $\alpha = 0.09$. (b) $\alpha = 0.19$. (c) $\alpha = 0.29$. (d) $\alpha = 0.39$. (e) $\alpha = 0.49$. (f) $\alpha = 0.59$. (g) $\alpha = 0.69$. (h) $\alpha = 0.79$. (i) $\alpha = 0.89$. (j) $\alpha = 0.99$.

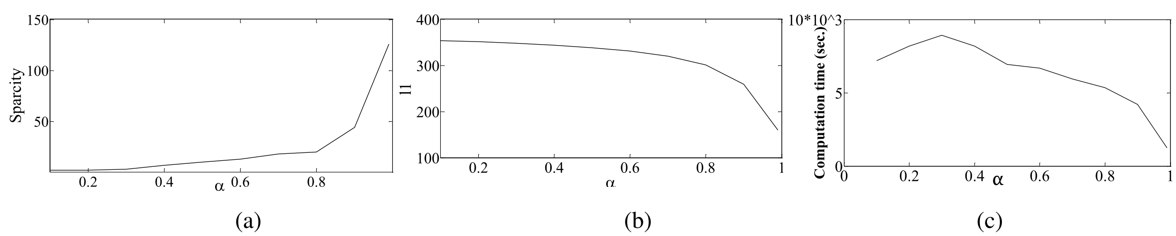

Fig. 7. Variation of parameters with user defined parameters α at a single pixel in the image. (a) Sparsity variation with α. (b) l_1-norm variation with α. (c) Computation time variation with α.

where ϕ is the phase, f_0 is the initial frequency, k is the rate of frequency change, and $f(t)$ is the instantaneous frequency. The thermal diffusion length corresponding to the excitation frequency range is depicted in Table I. Thermal diffusion length is defined as the distance over which the amplitude of thermal waves reduces to $(1/e\text{th})$ of its surface and is calculated by the following equation:

$$\mu(t) = \sqrt{\frac{2 \times \ k}{\omega(t)\rho c}} \tag{14}$$

where μ is the thermal diffusion length, k is the thermal conductivity, $\upsilon =$ is the excitation frequency, $\omega(t)$ (angular frequency) $= 2\pi f(t)$, $\rho =$ density, and $c =$ specific heat. Equation (14) depicts the variation of diffusion length with excitation frequency as a function of time.

B. Setup

Fig. 3 depicts the experimental setup. The setup comprises of an infrared camera, a test piece, an excitation LED source with modulation circuitry, a reference signal acquisition setup, and a computer. The complete setup is described in detail in [10]. A commercially available 40-W LED is used as an excitation source. The LED works with a driver that converts the in-line voltage to a 40-V 1-A dc LED driving voltage. The LED is modulated by turning on–off through a relay which is controlled by a microcontroller. The modulation in LED is recorded with a light detecting resistor (LDR) and forms the reference signal and the dictionary in processing part. The recorded signal from LDR is processed with an LM323 comparator to generate a digital level output against a voltage that is adjusted with a 10-k potentiometer.

The test piece is a carbon fiber reinforced polymer (CFRP) sample with artificially drilled cylindrical holes. The schematic of CFRP sample is shown in Fig. 2. The sample is 7 mm thick with 4- and 6-mm defect diameter, and defect depth varying from 0.25 to 2.5 mm in 0.25-mm increment. The sample is subjected to an impact damage at the center.

A FLIR SC5000M 14-bit infrared camera is used in the experiment with a resolution of 320×240 pixels and a spectral range of 2.5–5.1 μm. The video is recorded in external trigger mode to maintain a time synchronization of LED excitation, reference signal capture, and thermal response video of the test piece for a duration of 1000 s. The frames are captured at a rate of 1 fps with a camera integration time of 1048 μs that corresponds to 5 °C–42 °C temperature range. The recorded video is stored in .ptw format and processed offline with different processing techniques described in subsequent sections.

V. Result and Discussion

A. Quadratic Frequency Modulation

Fig. 4 depicts normalized timing diagram of compressed pulse for defects with varying depth. Fig. 4(b) shows that pulse peak time for each defect varies with defect depth. Thus, the quantification of defects would require a multiple frame data analysis. Fig. 5 shows thermograms for selected frames from pulse compressed video for a quadratic frequency modulated signal. The figure shows deeper defects appear later in time. This is in agreement with Fig. 4(b) and earlier reported pulse thermography work [16].

B. Sparse Algorithm

The sparse algorithm has been described in Section III-A. In (5), $x[n]$ is a 1×1000 column matrix representing temperature variation obtained from the IR camera at a pixel. The dictionary ψ is a time-shifted version of reference signal recorded with an LDR and has a dimension of 1000×200. The resultant Fig. 6 depicts the thermal images obtained with LASSO at different initial values of α. The figure further shows sparse coefficient variation with time for a pixel with defect and marked in white. Fig. 7(a) shows the variation in sparsity of sparse coefficients in Fig. 10. Sparsity, herein, is defined as the number of zeros in the sparse matrix and found to rise with α in Fig. 7(a). Furthermore, l_1 norm in Fig. 7(b) is defined as $\sum_{i=1}^{N} |\theta_i|$, where θ is sparse coefficient in Fig. 10 for index i. The figure shows l_1-norm to reduce monotonically with α. The change in computation time with

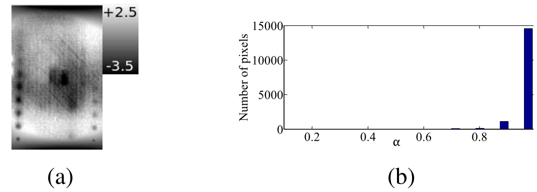

Fig. 8. Results from optimized α algorithm. (a) Thermal Image. (b) Histogram depicting α for number of pixels.

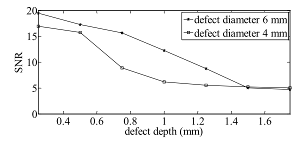

Fig. 9. SNR variation with defect depth for cross-correlated video.

α is depicted in Fig. 7(c). The computation time is minimum for α at 0.99. Sparsity is maximum and l_1-norm is minimum at this α value.

Fig. 8 depicts a resultant thermal image obtained by optimizing α with algorithm described in Section III-B. The histogram plot shows number of pixels with different values of optimized α used in the algorithm. α with 0.99 value is used for maximum number of pixels. α is optimized for a given pixel by minimization of cross-validation error as is depicted in Section III-B. α between 0.01 and 0.6 is not considered by any of the pixels as an optimized value with the mentioned algorithm.

C. SNR Calculation

The SNR calculation for a compressed pulse video with a different set of defects in a thermal image is calculated by a sequence of steps. For a particular defect, the SNR algorithm is applied on a specific frame or thermograms as per the occurrence of pulse peak time from Fig. 4.

1) The surface nonuniformity in thermal images are removed by third-order surface fitting. The resultant nonuniformity removed image is used for further processing.
2) *Signal Generation:* Each defect location is individually identified and fit with a Gaussian surface. The amplitude of the Gaussian fit surface is defined as a signal.
3) *Noise Generation:* A signal location is defined by a logical argument that states that a pixel value, greater than the standard deviation between fit surface and raw image is defined as a signal. The identified signal location is zeroed, and remaining pixels are used for calculation of rms noise.

Fig. 9 depicts SNR variation with defect depth for defects with diameter 6 and 4 mm, respectively. The figure shows the SNR to reduce with defect depth. This is attributed to the attenuation of thermal waves with depth. The thermal wave propagation phenomenon is described in Section IV. Furthermore, the SNR of defect with diameter 4 mm is much lower and follows from 3-D diffusion of thermal waves, described in [40].

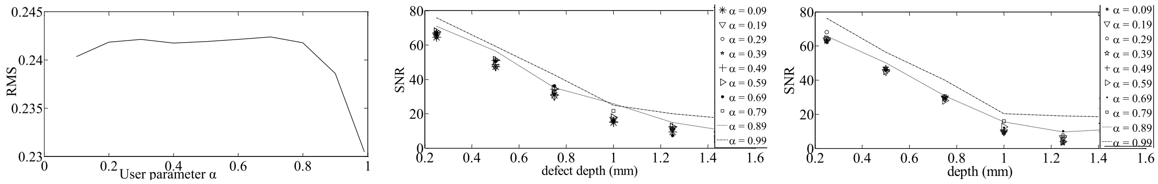

Fig. 10. Variation of thermal image SNR parameters with α. (a) RMS background noise in thermal images variation with α. (b) SNR variation with defect depth for a defect diameter 4 mm. (c) SNR variation with defect depth for a defect diameter 6 mm.

The image quality of resultant thermal images in Fig. 10 is determined by its SNR value. Fig. 10(a) depicts the variation in background rms noise of thermal images in Fig. 10 with α. The SNR variation with defect depth for different α is depicted in Fig. 10(b) and (c). The figures show that SNR curve follows the same trend as in Fig. 9 and reduces monotonically with defect depth. The SNR for each of the defects is the maximum at α 0.99. This follows from the fact that the rms noise in Fig. 10(a) is minimum at 0.99 and found to reduce with α.

D. Defect Diameter Estimation

The defect diameter estimation method follows from the SNR calculation algorithm in Section V-C. The Gaussian surface fitting on each individual defect is illustrated in the following equation:

$$g(x, y) = A \exp\left(-\left(\frac{x - x_0}{2s_x}\right)^2 - \left(\frac{y - y_0}{2s_y}\right)^2\right) \quad (15)$$

where A is the amplitude of the Gaussian surface, x_0 and y_0 represent the center of the Gaussian surface peak, s_x and s_y represent the standard deviation and determine the width of the Gaussian curve along x- and y-axes, respectively. For a cross correlation algorithm, the gauss fitting method is a multiframe process. A defect diameter is estimated for a frame with pulse peak time that varies for each defect. The pulse peak time for each defect is depicted in Fig. 4.

A Gaussian surface is a 3-D representation for a circular defect, with x_0 and y_0 representing the center point of the defect, and s_x and s_y representing the diameter of the defect along the x- and y-directions. Fig. 11 depicts the apparent defect diameter for 4- and 6-mm defects with cross correlation and sparse reconstruction algorithm. The defect diameter is defined as twice the average of s_x and s_y. The figure shows that the defect diameter appears larger for cross correlation algorithm when compared with sparse algorithm. This proves that the sparse reconstruction is a useful processing tool for detection and resolution of two closely spaced defects. Furthermore, the image shows an apparent rise in defect diameter with depth. This is attributed to a reduction in defect amplitude with depth that leads to a flatter gauss fit. Hence, defect diameter estimation varies as a function of defect depth, and a prior knowledge of defect depth is required for its accurate diameter estimation. However, it is important to mention that the accuracy of measurement of s_x and s_y for a fit surface is highly dependent on the initial gauss surface fit values.

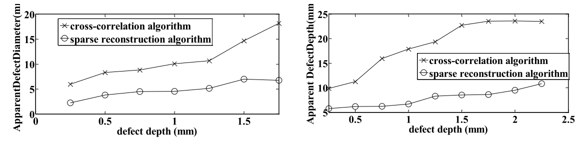

Fig. 11. Defect diameter estimation for defects with diameter (a) 4 mm and (b) 6 mm with cross correlation and sparse reconstruction algorithm. (a) Defect diameter - 4 mm. (b) Defect diameter −6 mm.

VI. Conclusion

This paper proposes and implements the application of sparse reconstruction method on thermal imaging for defect detection. This paper further compares the aforementioned processing tool with established cross correlation in the area of thermal imaging defect detection to draw specific conclusions. A sparse reconstruction tool generates an image, thus compressing a 4.08-GB compressed pulse video to a few kB. The memory efficient processing tool further simplifies the data analysis, when compared with complex cross-correlated video output.

The variation in sparse reconstruction coefficients with user parameter α is studied and found that the number of nonzero component, l_1-norm, and computation time reduces considerably at $\alpha = 0.9$ and 0.99. Furthermore, SNR for defects with varying depth is much larger for α with value 0.9 and 0.99. This is due to considerably less background noise at aforementioned α. Furthermore, the SNR for sparse reconstruction is much higher, when compared with cross correlation method.

An algorithm is formulated to optimize α and is selected with a minimum cross-validation error, which is calculated with tenfold cross-validation problem. The algorithm is individually used on each pixel. The resultant sparse reconstructed and cross-correlated images are tested for quantifying defect diameters. The apparent defect diameters are found to vary with defect depth. Compared to cross correlation algorithm, results show lower defect enlargement with the sparse algorithm. This concludes that sparse reconstruction is useful for resolving multiple close-spaced defects.

References

[1] G. Busse, D. Wu, and W. Karpen, "Thermal wave imaging with phase sensitive modulated thermography," *J. Appl. Phys.*, vol. 71, no. 8, pp. 3962–3965, Jan. 1992.

[2] D. Roy, K. Chatterjee, and S. Tuli, "Characterization and energy absorption efficiency determination of LED as an effective photothermal excitation source in lock-in thermography," *IEEE Sensors J.*, vol. 15, no. 10, pp. 6010–6016, Oct. 2015.

[3] R. Mulaveesala and S. Tuli, "Theory of frequency modulated thermal wave imaging for nondestructive subsurface defect detection," *Appl. Phys. Lett.*, vol. 89, no. 19, p. 191913, 2006.

[4] K. Chatterjee, S. Tuli, S. G. Pickering, and D. P. Almond, "A comparison of the pulsed, lock-in and frequency modulated thermography nondestructive evaluation techniques," *NDT&E Int.*, vol. 44, no. 7, pp. 655-667, 2011.

[5] J. R. Klauder, A. C. Price, S. Darlington, and W. J. Albersheim, "The theory and design of chirp radars," *Bell Syst. Tech. J.*, vol. 39, no. 4, pp. 745–808, Jul. 1960.

[6] S. Tuli and R. Mulaveesala, "Defect detection by pulse compression in frequency modulated thermal wave imaging," *Quant. InfraRed Thermogr. J.*, vol. 2, no. 1, pp. 41–54, 2005.

[7] R. Mulaveesala, J. S. Vaddi, and P. Singh, "Pulse compression approach to infrared nondestructive characterization," *Rev. Sci. Instrum.*, vol. 79, no. 9, p. 094901, 2008.

[8] V. S. Ghali and R. Mulaveesala, "Comparative data processing approaches for thermal wave imaging techniques for non-destructive testing," *Sens. Imag., Int. J.*, vol. 12, nos. 1–2, pp. 15–33, 2011.

[9] K. Chatterjee, D. Roy, and S. Tuli, "A novel pulse compression algorithm for frequency modulated active thermography using band-pass filter," *Infr. Phys. Technol.*, vol. 82, pp. 75–84, May 2017.

[10] D. Roy and S. Tuli, "Applicability of LED-based excitation source for defect depth resolved frequency modulated thermal wave imaging," *IEEE Trans. Instrum. Meas.*, vol. 66, no. 10, pp. 2658–2665, Oct. 2017.

[11] L. Fang and S. Li, "Face recognition by exploiting local Gabor features with multitask adaptive sparse representation," *IEEE Trans. Instrum. Meas.*, vol. 64, no. 10, pp. 2605–2615, Oct. 2015.

[12] H. Liu, D. Guo, and F. Sun, "Object recognition using tactile measurements: Kernel sparse coding methods," *IEEE Trans. Instrum. Meas.*, vol. 65, no. 3, pp. 656–665, Mar. 2016.

[13] L. Fang, C. Wang, S. Li, and J. A. Benediktsson, "Hyperspectral image classification via multiple-feature-based adaptive sparse representation," *IEEE Trans. Instrum. Meas.*, vol. 66, no. 7, pp. 1646–1657, Jul. 2017.

[14] P. R. Muduli and A. Mukherjee, "A subspace projection-based joint sparse recovery method for structured biomedical signals," *IEEE Trans. Instrum. Meas.*, vol. 66, no. 2, pp. 234–242, Feb. 2017.

[15] D. P. Almond and S. K. Lau, "Defect sizing by transient thermography. I. An analytical treatment," *J. Phys. D, Appl. Phys.*, vol. 27, no. 5, p. 1063, 1994.

[16] V. P. Vavilov and D. D. Burleigh, "Review of pulsed thermal NDT: Physical principles, theory and data processing," *NDT&E Int.*, vol. 73, pp. 28-52, Jul. 2015.

[17] P. Charbonnier, L. Blanc-Feraud, G. Aubert, and M. Barlaud, "Deterministic edge-preserving regularization in computed imaging," *IEEE Trans. Image Process.*, vol. 6, no. 2, pp. 298–311, Feb. 1997.

[18] B. Yang and S. Li, "Multifocus image fusion and restoration with sparse representation," *IEEE Trans. Instrum. Meas.*, vol. 59, no. 4, pp. 884–892, Apr. 2010.

[19] J. Ye, H. Wang, and W. Yang, "Image reconstruction for electrical capacitance tomography based on sparse representation," *IEEE Trans. Instrum. Meas.*, vol. 64, no. 1, pp. 89–102, Jan. 2015.

[20] F. Soldovieri, R. Solimene, L. L. Monte, M. Bavusi, and A. Loperte, "Sparse reconstruction from GPR data with applications to Rebar detection," *IEEE Trans. Instrum. Meas.*, vol. 60, no. 3, pp. 1070–1079, Mar. 2011.

[21] M. J. Hasankhan, S. Samadi, and M. Çetin, "Sparse representation-based algorithm for joint SAR image formation and autofocus," *Signal, Image Video Process.*, vol. 11, no. 4, pp. 589–596, 2017.

[22] X. Zhu, G. Jin, F. He, and Z. Dong, "Radar imaging of sidelobe suppression based on sparse regularization," *J. Comput. Commun.*, vol. 4, no. 3, pp. 108–115, 2016.

[23] B. Wu, Y. Huang, and S. Krishnaswamy, "A Bayesian approach for sparse flaw detection from noisy signals for ultrasonic NDT," *NDT&E Int.*, vol. 85, pp. 76–85, Jan. 2017.

[24] M. Ricci *et al.*, "Exploiting non-linear chirp and sparse deconvolution to enhance the performance of pulse-compression ultrasonic NDT," in *Proc. IEEE Int. Ultrason. Symp.*, Oct. 2012, pp. 1489–1492.

[25] S. Hamidi and S. ShahbazPanahi, "Sparse signal recovery based imaging in the presence of mode conversion with application to non-destructive testing," *IEEE Trans. Signal Process.*, vol. 64, no. 5, pp. 1352–1364, Mar. 2016.

[26] P. O'Shea, "A fast algorithm for estimating the parameters of a quadratic FM signal," *IEEE Trans. Signal Process.*, vol. 52, no. 2, pp. 385–393, Feb. 2004.

[27] C. Yoon, Y. Yoo, T.-K. Song, and J. H. Chang, "Orthogonal quadratic chirp signals for simultaneous multi–zone focusing in medical ultrasound imaging," *IEEE Trans. Ultrason., Ferroelectr., Freq. Control*, vol. 59, no. 5, pp. 1061–1069, May 2012.

[28] G. V. Subbarao and R. Mulaveesala, "Quadratic frequency modulated thermal wave imaging for non-destructive testing," *Prog. Electromagn. Res. M*, vol. 26, pp. 11–22, 2012.

[29] A. C. Pecci, C. Laot, and A. Bourre, "Quadratic chirp modulation for underwater acoustic digital communications," in *Proc. OCEANS*, May 2015, pp. 1–7.

[30] E. J. Candès, "Compressive sampling," in *Proc. Int. Congr. Math.*, vol. 3, 2006, pp. 1433–1452.

[31] K. R. Varshney, M. Çetin, J. W. Fisher, and A. S. Willsky, "Sparse representation in structured dictionaries with application to synthetic aperture radar," *IEEE Trans. Signal Process.*, vol. 56, no. 8, pp. 3548–3561, Aug. 2008.

[32] A. Lazarov, H. Kabakchiev, T. Kostadinov, and D. Minchev, "GISAR image reconstruction based 2-D smoothed l0 norm minimization in sparse decomposition," in *Proc. 16th Int. Radar Symp. (IRS)*, Jun. 2015, pp. 416–421.

[33] S. S. Chen, D. L. Donoho, and M. A. Saunders, "Atomic decomposition by basis pursuit," *SIAM J. Sci. Comput.*, vol. 43, no. 1, pp. 129–159, 1999.

[34] P. R. Gill, A. Wang, and A. Molnar, "The in-crowd algorithm for fast basis pursuit denoising," *IEEE Trans. Signal Process.*, vol. 59, no. 10, pp. 4595–4605, Oct. 2011.

[35] P. Boufounos, M. F. Duarte, and R. G. Baraniuk, "Sparse signal reconstruction from noisy compressive measurements using cross validation," in *Proc. IEEE/SP 14th Workshop Stat. Signal Process.*, Aug. 2007, pp. 299–303.

[36] J. A. K. Suykens, J. De Brabanter, L. Lukas, and J. Vandewalle, "Weighted least squares support vector machines: Robustness and sparse approximation," *Neurocomputing*, vol. 48, nos. 1–4, pp. 85–105, 2002.

[37] G. C. Cawley and N. L. C. Talbot, "Fast exact leave-one-out cross-validation of sparse least-squares support vector machines," *Neural Netw.*, vol. 17, no. 10, pp. 1467–1475, 2004.

[38] M. J. Wainwright, "Sharp thresholds for high-dimensional and noisy sparsity recovery using ℓ_1-constrained quadratic programming (Lasso)," *IEEE Trans. Inf. Theory*, vol. 55, no. 5, pp. 2183–2202, May 2009.

[39] I. Drori and D. L. Donoho, "Solution of ℓ_1 minimization problems by LARS/homotopy methods," in *Proc. IEEE Int. Conf. Acoust. Speech Signal Process.*, vol. 3, May 2006, p. 3.

[40] K. Chatterjee and S. Tuli, "Prediction of blind frequency in lock-in thermography using electro-thermal model based numerical simulation," *J. Appl. Phys.*, vol. 114, no. 17, pp. 174905-1–174905-8, 2013.

Deboshree Roy received the B.Sc. degree (Hons.) in physics from Delhi University, New Delhi, India, in 2007, the M.Sc. degree in physics (major in electronics) from the Kirori Mal College, Delhi University, in 2009, and the M.Tech. degree in instrumentation from the National Institute of Technology, Kurukshetra, India, in 2011. She is currently pursuing the Ph.D. degree from the Centre of Applied Research in Electronics, IIT Delhi, New Delhi.

Her current research interests include thermal wave imaging nondestructive testing and signal processing.

Prabhu Babu received the B.Tech. degree in electronics from the Madras Institute of Technology, Chennai, India, in 2005, the M.Tech. degree in radio frequency design technology from the Centre for Applied Research in Electronics (CARE), IIT Delhi, New Delhi, India, in 2007, and the Ph.D. degree in philosophy from Uppsala University, Uppsala, Sweden, in 2012.

From 2013 to 2015, he was with the Hong Kong University of Science and Technology, Hong Kong, where he was doing his postdoctoral research. In 2016, he joined CARE, IIT Delhi, as an Assistant Professor.

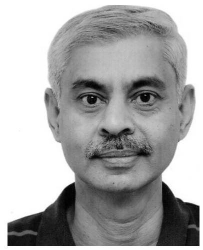

Suneet Tuli received the B.E. degree (Hons.) in electrical and electronics engineering from the Birla Institute of Technology and Science (BITS), Pilani, India, in 1982, and the M.Tech. and Ph.D. degrees in electronics engineering from IIT Delhi, New Delhi, India.

Since 1986, he has been a Faculty Member with the Centre for Applied Research in Electronics (CARE), IIT Delhi, where he was the Head from 2009 to 2012. From 2012 to 2016, he was the Dean of the Research and Development Centre, IIT Delhi, where he was the Associate Dean from 2005 to 2009. He has been a Visiting Researcher with the University of Bath, Bath, U.K. and also the University of Piere et Marie Curie, Paris, France. He has been involved in surface acoustic wave devices design and technology. His current research interests include thermo-acoustic-optical interaction and active and passive thermography for nondestructive characterization systems.

Dr. Tuli was a recipient of the 10th IETE Professor K. Sreenivas Memorial Award for distinguished teaching in 2003. He is on the editorial boards of *Quantitative Infrared Thermography Journal* and the *IETE Journal of Research*.